

On the analysis and interpretation of inhomogeneous quadratic forms as receptive fields

Pietro Berkes and Laurenz Wiskott

Institute for Theoretical Biology

Humboldt University Berlin

Invalidenstraße 43, D-10115 Berlin, Germany

{p.berkes,l.wiskott}@biologie.hu-berlin.de

<http://itb.biologie.hu-berlin.de/~berkes,~wiskott>

Abstract

In this paper we introduce some mathematical and numerical tools to analyze and interpret inhomogeneous quadratic forms. The resulting characterization is in some aspects similar to that given by experimental studies of cortical cells, making it particularly suitable for application to second-order approximations and theoretical models of physiological receptive fields. We first discuss two ways of analyzing a quadratic form by visualizing the coefficients of its quadratic and linear term directly and by considering the eigenvectors of its quadratic term. We then present an algorithm to compute the optimal excitatory and inhibitory stimuli, i.e. the stimuli that maximize and minimize the considered quadratic form, respectively, given a fixed energy constraint. The analysis of the optimal stimuli is completed by considering their invariances, which are the transformations to which the quadratic form is most insensitive. We introduce a test to determine which of these are statistically significant. Next we propose a way to measure the relative contribution of the quadratic and linear term to the total output of the quadratic form. Furthermore, we derive simpler versions of the above techniques in the special case of a quadratic form without linear term and discuss the analysis of such functions in previous theoretical and experimental studies. In the final part of the paper we show that for each quadratic form it is possible to build an equivalent two-layer neural network, which is compatible with (but more general than) related networks used in some recent papers and with the energy model of complex cells. We show that the neural network is unique only up to an arbitrary orthogonal transformation of the excitatory and inhibitory subunits in the first layer.

Keywords: Quadratic forms, receptive fields, nonlinear analysis, visualization.

1 Introduction

Recent research in neuroscience has seen an increasing number of extensions of established linear techniques to their nonlinear equivalent, in both experimental and theoretical studies. This is the case, for example, for spatio-temporal receptive-field estimates in physiological studies (e.g. [Toussaint et al., 2002](#); [Rust et al., 2004](#)) and information theoretical models like principal component analysis (PCA) ([Schölkopf et al., 1998](#)) and independent component analysis (ICA) (see ([Jutten and Karhunen, 2003](#)) for a review). Additionally, new nonlinear unsupervised algorithms have been introduced, like, for example, slow feature analysis (SFA) ([Wiskott and Sejnowski, 2002](#)). The study of the resulting nonlinear functions can be a difficult task because of the lack of appropriate tools to characterize them qualitatively and quantitatively.

During a recent project concerning the self-organization of complex-cell receptive fields in the primary visual cortex (V1) ([Berkes and Wiskott, 2002, 2003](#), see Sect. 2) we have developed some of these tools to analyze quadratic functions in a high-dimensional space. Because of the complexity of the methods we describe them here in a separate paper. The resulting characterization is in some aspects similar to that given by physiological studies, making it particularly suitable to be applied to the analysis of nonlinear receptive fields.

We are going to focus on the analysis of the inhomogeneous quadratic form

$$g(\mathbf{x}) = \frac{1}{2}\mathbf{x}^T\mathbf{H}\mathbf{x} + \mathbf{f}^T\mathbf{x} + c, \quad (1)$$

where \mathbf{x} is an N -dimensional input vector, \mathbf{H} an $N \times N$ matrix, \mathbf{f} an N -dimensional vector, and c a constant. Although some of the mathematical details of this study are specific to quadratic forms only, it should be straightforward to extend most of the methods to other nonlinear functions while preserving the same interpretations. In other contexts it might be more useful to approximate the functions under consideration by a quadratic form using a Taylor expansion up to the second order and then apply the algorithms described here.

Table 1 lists some important terms and variables used throughout the paper. We will refer to $\frac{1}{2}\mathbf{x}^T\mathbf{H}\mathbf{x}$ as the *quadratic term*, to $\mathbf{f}^T\mathbf{x}$ as the *linear term* and to c as the *constant term* of the quadratic form. Without loss of generality we assume that \mathbf{H} is a symmetric matrix, since if necessary we can substitute \mathbf{H} in Equation (1) by the symmetric matrix $\frac{1}{2}(\mathbf{H} + \mathbf{H}^T)$ without changing the values of the function g . We define μ_1, \dots, μ_N to be the eigenvalues to the eigenvectors $\mathbf{v}_1, \dots, \mathbf{v}_N$ of \mathbf{H} , sorted in decreasing order $\mu_1 \geq \mu_2 \geq \dots \geq \mu_N$. $\mathbf{V} = (\mathbf{v}_1, \dots, \mathbf{v}_N)$ denotes the matrix of the eigenvectors and \mathbf{D} the diagonal matrix of the corresponding eigenvalues, so that $\mathbf{V}^T\mathbf{H}\mathbf{V} = \mathbf{D}$. Furthermore, $\langle \cdot \rangle_t$ indicates the mean over time of the expression included in the angle brackets.

| | |
|------------------------------|--|
| N | Number of dimensions of the input space. |
| $\langle \cdot \rangle_t$ | Mean over time of the expression between the two brackets. |
| \mathbf{x} | Input vector. |
| g, \tilde{g} | The considered inhomogeneous quadratic form and its restriction to a sphere. |
| \mathbf{H}, \mathbf{h}_i | $N \times N$ matrix of the quadratic term of the inhomogeneous quadratic form (Eq. 1) and i -th row of \mathbf{H} (i.e. $\mathbf{H} = (\mathbf{h}_1, \dots, \mathbf{h}_N)^T$). \mathbf{H} is assumed to be symmetric. |
| \mathbf{v}_i, μ_i | i -th eigenvector and eigenvalue of \mathbf{H} , sorted by decreasing eigenvalues (i.e. $\mu_1 \geq \mu_2 \geq \dots \geq \mu_N$). |
| \mathbf{V}, \mathbf{D} | The matrix of the eigenvectors $\mathbf{V} = (\mathbf{v}_1, \dots, \mathbf{v}_N)$ and the diagonal matrix of the eigenvalues, such that $\mathbf{V}^T\mathbf{H}\mathbf{V} = \mathbf{D}$. |
| \mathbf{f} | N -dimensional vector of the linear term of the inhomogeneous quadratic form (Eq. 1). |
| c | Scalar value of the constant term of the inhomogeneous quadratic form (Eq. 1). |
| $\mathbf{x}^+, \mathbf{x}^-$ | Optimal excitatory and inhibitory stimuli, $\ \mathbf{x}^+\ = \ \mathbf{x}^-\ = r$. |

Table 1 Definition of some important terms This table lists the definition of the most important terms and the basic assumptions of the paper.

In the next section we introduce the model system that we are going to use for illustration throughout this paper. Section 3 describes two ways of analyzing a quadratic form by visualizing the coefficients of its quadratic and linear term directly and by considering the eigenvectors of its quadratic term. We then present in Section 4 an algorithm to compute the optimal excitatory and inhibitory stimuli, i.e. the stimuli that maximize and minimize a quadratic form, respectively, given a fixed energy constraint. In Section 5 we consider the invariances of the optimal stimuli, which are the transformations to which the function is most insensitive, and in the following section we introduce a test to determine which of these are statistically significant. In Section 7 we discuss two ways to determine the relative contribution of the different terms of a quadratic form to its output. Furthermore, in Section 8 we consider the techniques described above in the special case of a quadratic form without the linear term. In the end we present in Section 9 a two-layer neural network architecture equivalent to a given quadratic form.

2 Model system

To illustrate the analysis techniques presented here we make use of the quadratic forms presented in (Berkes and Wiskott, 2002) in the context of a theoretical model of self-organization of complex-cell receptive fields

in the primary visual cortex (see also [Berkes and Wiskott, 2003](#)). In this section we summarize the settings and main results of this example system.

We generated image sequences from a set of natural images by moving an input window over an image by translation, rotation, and zoom and subsequently rescaling the collected stimuli to a standard size of 16×16 pixels. For efficiency reasons the dimensionality of the input vectors \mathbf{x} was then reduced from 256 to 50 input dimensions including a whitening using principal component analysis (PCA) with

$$\mathbf{x}' = \mathbf{W}(\mathbf{x} - \langle \mathbf{x} \rangle_t), \quad (2)$$

with \mathbf{W} being a 50×256 -matrix. We then determined quadratic forms (or *units*) by applying SFA to the input data. SFA is an implementation of the *temporal slowness principle* (see ([Wiskott and Sejnowski, 2002](#)) and references therein): given a finite dimensional function space, SFA extracts the functions that, applied to the input data, return output signals that vary as slowly as possible in time as measured by the variance of the first derivative under the constraint that the output signals have zero mean, unit variance, and are decorrelated. The functions are sorted by decreasing slowness.

Under an affine transformation of the coordinates $\mathbf{x}' = \mathbf{A}\mathbf{x} + \mathbf{b}$ the quadratic form

$$g(\mathbf{x}') = \frac{1}{2} \mathbf{x}'^T \mathbf{H}' \mathbf{x}' + \mathbf{f}'^T \mathbf{x}' + c' \quad (3)$$

becomes

$$g(\mathbf{A}\mathbf{x} + \mathbf{b}) = \frac{1}{2} (\mathbf{A}\mathbf{x} + \mathbf{b})^T \mathbf{H}' (\mathbf{A}\mathbf{x} + \mathbf{b}) + \mathbf{f}'^T (\mathbf{A}\mathbf{x} + \mathbf{b}) + c' \quad (4)$$

$$= \frac{1}{2} \mathbf{x}^T \mathbf{A}^T \mathbf{H}' \mathbf{A} \mathbf{x} + \mathbf{b}^T \mathbf{H}' \mathbf{A} \mathbf{x} + \frac{1}{2} \mathbf{b}^T \mathbf{H}' \mathbf{b} + \mathbf{f}'^T \mathbf{A} \mathbf{x} + \mathbf{f}'^T \mathbf{b} + c' \quad (5)$$

$$= \frac{1}{2} \mathbf{x}^T (\mathbf{A}^T \mathbf{H}' \mathbf{A}) \mathbf{x} + (\mathbf{A}^T \mathbf{H}' \mathbf{b} + \mathbf{A}^T \mathbf{f}')^T \mathbf{x} + \left(\frac{1}{2} \mathbf{b}^T \mathbf{H}' \mathbf{b} + \mathbf{f}'^T \mathbf{b} + c' \right) \quad (6)$$

$$=: \frac{1}{2} \mathbf{x}^T \mathbf{H} \mathbf{x} + \mathbf{f}^T \mathbf{x} + c, \quad (7)$$

i.e. another quadratic form. For analysis we can thus project the learned functions back into the input space applying Equations (4-7) with $\mathbf{A} := \mathbf{W}$ and $\mathbf{b} := -\mathbf{W}\langle \mathbf{x}' \rangle_t$. Note that the rank of the quadratic term \mathbf{H} after the transformation is the same as before and it has only 50 eigenvectors.

The units receive visual stimuli as input and can thus be interpreted as nonlinear receptive fields. They were analyzed with the algorithms presented here and with sine-grating experiments similar to the ones performed in physiology and were found to reproduce many properties of complex cells in V1, not only the primary ones, i.e. response to edges and phase-shift invariance (see Sects. 4 and 5), but also a range of secondary ones such as direction selectivity, non-orthogonal inhibition, end-inhibition, and side-inhibition.

This model system is complex enough to require an extensive analysis and is representative of the application domain considered here, which includes second-order approximations and theoretical models of physiological receptive fields.

3 Visualization of coefficients and eigenvectors

One way to analyze a quadratic form is to look at its coefficients. The coefficients f_1, \dots, f_N of the linear term can be visualized and interpreted directly. They give the shape of the input stimulus that maximizes the linear part given a fixed norm.

The quadratic term can be interpreted as a sum over the inner product of the j -th row \mathbf{h}_j of \mathbf{H} with the vector of the products $x_j x_i$ between the j -th variable x_j and all other variables:

$$\mathbf{x}^T \mathbf{H} \mathbf{x} = \sum_{j=1}^N x_j (\mathbf{h}_j^T \mathbf{x}) = \sum_{j=1}^N \mathbf{h}_j^T \begin{pmatrix} x_j x_1 \\ x_j x_2 \\ \vdots \\ x_j x_N \end{pmatrix}. \quad (8)$$

In other words, the response of the quadratic term is formed by the sum of N linear filters \mathbf{h}_j which respond to all combinations of the j -th variable with the other ones.

If the input data has a two-dimensional spatial arrangement, like in our model system, the interpretation of the rows can be made easier by visualizing them as a series of images (by reshaping the vector \mathbf{h}_j to match the structure of the input) and arranging them according to the spatial position of the corresponding variable x_j . In Figure 1 we show some of the coefficients of two functions learned in the model system. In both units, the linear term looks unstructured. The absolute values of its coefficients are small in comparison to those of the quadratic term so that its contribution to the output of the functions is very limited (cf. Sect. 7). The row vectors \mathbf{h}_j of Unit 4 have a localized distribution of their coefficients, i.e. they only respond to combinations of the corresponding variable x_j and its neighbors. The filters \mathbf{h}_j are shaped like a four-leaf clover and centered on the variable itself. Pairs of opposed leaves have positive and negative values, respectively. This suggests that the unit responds to stimuli oriented in the direction of the two positive leaves and is inhibited by stimuli with an orthogonal orientation, which is confirmed by successive analysis (cf. later in this section and Sect. 4). In Unit 28 the appearance of \mathbf{h}_j depends on the spatial position of \mathbf{x}_j . In the bottom half of the receptive field the interaction of the variables with their close neighbors along the vertical orientation is weighted positively, with a negative flank on the sides. In the top half the rows have similar coefficients but with reversed polarity. As a consequence, the unit responds strongly to vertical edges in the bottom half, while vertical edges in the top half result in strong inhibition. Edges extending over the whole receptive field elicit only a weak total response. Such a unit is said to be end-inhibited.

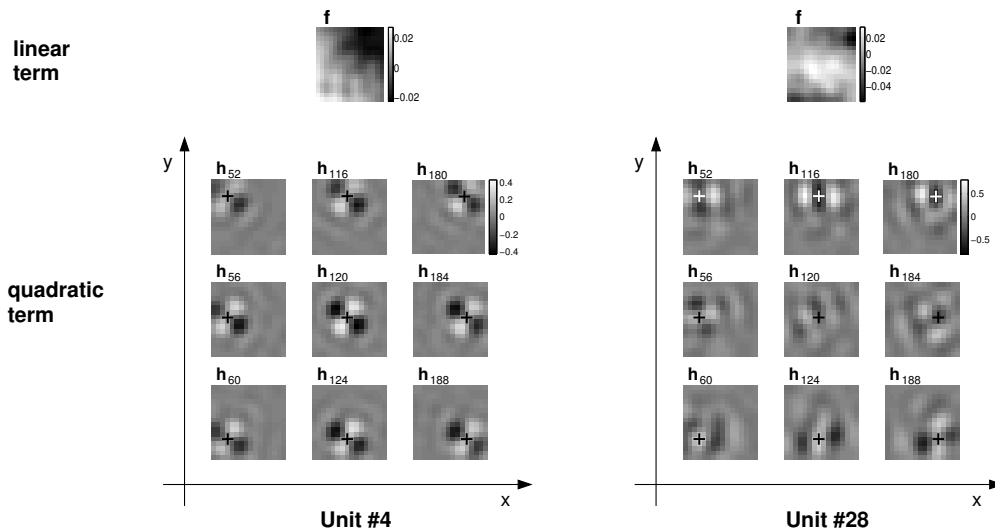


Figure 1 Quadratic form coefficients This figure shows some of the quadratic form coefficients of two functions learned in the model system. The top plots show the coefficients of the linear term \mathbf{f} , reshaped to match the two-dimensional shape of the input. The bottom plots show the coefficients of nine of the rows \mathbf{h}_j of the quadratic term. The crosses indicate the spatial position of the corresponding reference index j .

Another possibility to visualize the quadratic term is to display its eigenvectors. The output of the quadratic form to one of the eigenvectors equals half of the corresponding eigenvalue, since $\frac{1}{2}\mathbf{v}_i^T\mathbf{H}\mathbf{v}_i = \frac{1}{2}\mathbf{v}_i^T(\mu_i\mathbf{v}_i) = \frac{1}{2}\mu_i$. The first eigenvector can be interpreted as the stimulus that among all input vectors with norm 1 maximizes the output of the quadratic term. The j -th eigenvector maximizes the quadratic term in the subspace that excludes the previous $j - 1$ ones. In Figure 2 we show the eigenvectors of the two functions previously analyzed in Figure 1. In Unit 4 the first eigenvector looks like a Gabor wavelet (i.e. a sine grating multiplied by a Gaussian). The second eigenvector has the same form except for a 90 degree phase shift of the sine grating. Since the two eigenvalues have almost the same magnitude, the response of the quadratic term is similar for the two eigenvectors and also for linear combinations with constant norm 1. For this reason the quadratic term of this function has the main characteristics of complex cells in V1, namely a strong response to an oriented grating with an invariance to the phase of the grating. The last two eigenvectors, which correspond to the stimuli that minimize the quadratic term, are Gabor wavelets with orientation orthogonal to the first two. This means that the output of the quadratic term is inhibited by stimuli at an orientation orthogonal to the preferred one. A similar interpretation can be given in the case of Unit 28, although in this case the first and the last two eigenvalues have the same orientation but occupy two

different halves of the receptive field. This confirms that Unit 28 is end-inhibited. A direct interpretation of the remaining eigenvectors in the two functions is difficult (see also Sect. 8), although the magnitude of the eigenvalues shows that some of them elicit a strong response. Moreover, the interaction of the linear and quadratic terms to form the overall output of the quadratic form is not considered but cannot generally be neglected. The methods presented in the following sections often give a more direct and intuitive description of the quadratic forms.

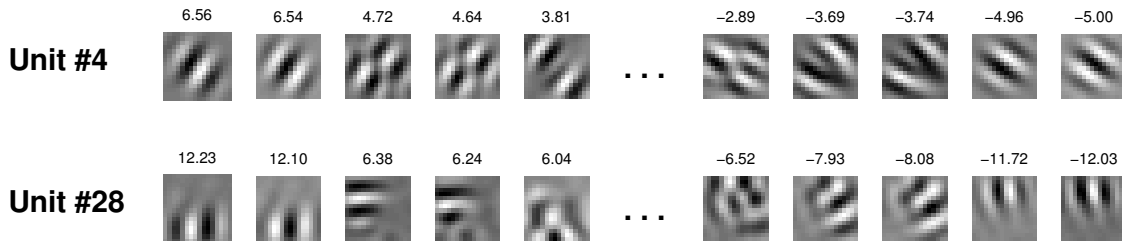


Figure 2 Eigenvectors of the quadratic term Eigenvectors of the quadratic term of two functions learned in the model system sorted by decreasing eigenvalues as indicated above each eigenvector.

4 Optimal stimuli

Another characterization of a nonlinear function can be borrowed from neurophysiological experiments, where it is common practice to characterize a neuron by the stimulus to which the neuron responds best (for an overview see Dayan and Abbott, 2001, chap. 2.2). Analogously, we can compute the *optimal excitatory stimulus* of g , i.e. the input vector \mathbf{x}^+ that maximizes g given a fixed norm $\|\mathbf{x}^+\| = r$. Note that \mathbf{x}^+ depends qualitatively on the value of r : if r is very small the linear term of the equation dominates, so that $\mathbf{x}^+ \approx \mathbf{f}$, while if r is very large the quadratic part dominates, so that \mathbf{x}^+ equals the first eigenvector of \mathbf{H} (see also Sect. 8). We usually choose r to be the mean norm of all input vectors, since we want \mathbf{x}^+ to be representative of the typical input. In the same way we can also compute the *optimal inhibitory stimulus* \mathbf{x}^- , which minimizes the response of the function.

The fixed norm constraint corresponds to a *fixed energy constraint* (Stork and Levinson, 1982) used in experiments involving the reconstruction of the Volterra kernel of a neuron (Dayan and Abbott, 2001, chap. 2.2). During physiological experiments in the visual system one sometimes uses stimuli with fixed contrast instead. The optimal stimuli under these two constraints may be different. For example, with fixed contrast one can extend a sine grating indefinitely in space without changing its intensity, while with fixed norm its maximum intensity is going to dim as the extent of the grating increases. The fixed contrast constraint is more difficult to enforce analytically (for example because the surface of constant contrast is not bounded).

The problem of finding the optimal excitatory stimulus under the fixed energy constraint can be mathematically formulated as follows:

$$\begin{array}{ll} \text{maximize} & g(\mathbf{x}) = \frac{1}{2}\mathbf{x}^T\mathbf{H}\mathbf{x} + \mathbf{f}^T\mathbf{x} + c \\ \text{under the constraint} & \mathbf{x}^T\mathbf{x} = r^2. \end{array} \quad (9)$$

This problem is known as the *Trust Region Subproblem* and has been extensively studied in the context of numerical optimization, where a nonlinear function is minimized by successively approximating it by an inhomogeneous quadratic form, which is in turn minimized in a small neighborhood. Numerous studies have analyzed its properties in particular in the numerically difficult case where \mathbf{H} is near to singular (see (Fortin, 2000) and references therein). We make use of some basic results and extend them where needed to fit our needs.

If the linear term is equal to zero (i.e. $\mathbf{f} = \mathbf{0}$), the problem can be easily solved (it is simply the first eigenvector scaled to norm r , see Sect. 8). In the following we consider the more general case where $\mathbf{f} \neq \mathbf{0}$.

We can use a Lagrange formulation to find the necessary conditions for the extremum:

$$\mathbf{x}^T \mathbf{x} = r^2 \quad (10)$$

$$\text{and } \nabla[g(\mathbf{x}) - \frac{1}{2}\lambda\mathbf{x}^T \mathbf{x}] = \mathbf{0} \quad (11)$$

$$\Leftrightarrow \mathbf{H}\mathbf{x} + \mathbf{f} - \lambda\mathbf{x} = \mathbf{0} \quad (12)$$

$$\Leftrightarrow \mathbf{x} = (\lambda\mathbf{I} - \mathbf{H})^{-1} \mathbf{f}, \quad (13)$$

where we inserted the factor $\frac{1}{2}$ for mathematical convenience. According to Theorem 3.1 in (Fortin, 2000), if an \mathbf{x} that satisfies Equation (13) is a solution to (9), then $(\lambda\mathbf{I} - \mathbf{H})$ is positive semidefinite (i.e. all eigenvalues are greater or equal to 0). This imposes a strong lower bound on the range of possible values for λ . Note that the matrix $(\lambda\mathbf{I} - \mathbf{H})$ has the same eigenvectors \mathbf{v}_i as \mathbf{H} with eigenvalues $(\lambda - \mu_i)$, since

$$(\lambda\mathbf{I} - \mathbf{H})\mathbf{v}_i = \lambda\mathbf{v}_i - \mathbf{H}\mathbf{v}_i \quad (14)$$

$$= \lambda\mathbf{v}_i - \mu_i\mathbf{v}_i \quad (15)$$

$$= (\lambda - \mu_i)\mathbf{v}_i. \quad (16)$$

For $(\lambda\mathbf{I} - \mathbf{H})$ to be positive semidefinite all eigenvalues must be nonnegative, and thus λ must be greater than the largest eigenvalue μ_1 ,

$$\mu_1 < \lambda. \quad (17)$$

An upper bound for lambda can be found by considering an upper bound for the norm of \mathbf{x} . First we note that matrix $(\lambda\mathbf{I} - \mathbf{H})^{-1}$ is symmetric and has the same eigenvectors as \mathbf{H} with eigenvalues $1/(\lambda - \mu_i)$:

$$(\lambda\mathbf{I} - \mathbf{H})\mathbf{v}_i \stackrel{(16)}{=} (\lambda - \mu_i)\mathbf{v}_i \quad (18)$$

$$\Leftrightarrow \frac{1}{(\lambda - \mu_i)}\mathbf{v}_i = (\lambda\mathbf{I} - \mathbf{H})^{-1}\mathbf{v}_i. \quad (19)$$

We also know that the inequality

$$\|\mathbf{A}\mathbf{v}\| \leq \|\mathbf{A}\|\|\mathbf{v}\| \quad (20)$$

holds for every matrix \mathbf{A} and vector \mathbf{v} . $\|\mathbf{A}\|$ is here the spectral norm of \mathbf{A} , which for symmetric matrices is simply the largest absolute eigenvalue. With this we find an upper bound for $\|\mathbf{x}\|$:

$$\|\mathbf{x}\| = \|(\lambda\mathbf{I} - \mathbf{H})^{-1}\mathbf{f}\| \quad (21)$$

$$\stackrel{(20)}{\leq} \|(\lambda\mathbf{I} - \mathbf{H})^{-1}\| \|\mathbf{f}\| \quad (22)$$

$$\stackrel{(19)}{=} \max_i \left\{ \left| \frac{1}{\lambda - \mu_i} \right| \right\} \|\mathbf{f}\| \quad (23)$$

$$\stackrel{(17)}{=} \frac{1}{\lambda - \mu_1} \|\mathbf{f}\|. \quad (24)$$

We can therefore discard all values of λ for which the upper bound is smaller than r (in which case the condition $\|\mathbf{x}\| = r$ would be violated), i.e. λ must fulfill the equation

$$r \leq \frac{1}{\lambda - \mu_1} \|\mathbf{f}\| \quad (25)$$

$$\Leftrightarrow \lambda \leq \frac{\|\mathbf{f}\|}{r} + \mu_1. \quad (26)$$

The optimization problem (9) is thus reduced to a search over λ on the interval $\left] \mu_1, \left(\frac{\|\mathbf{f}\|}{r} + \mu_1 \right) \right]$ until \mathbf{x} defined by (13) fulfills the constraint $\|\mathbf{x}\| = r$ (Eq. 10). Vector \mathbf{x} and norm $\|\mathbf{x}\|$ can be efficiently computed

for each λ using the eigenvalue decomposition of \mathbf{f} :

$$\mathbf{x} = (\lambda\mathbf{I} - \mathbf{H})^{-1}\mathbf{f} \quad (27)$$

$$= (\lambda\mathbf{I} - \mathbf{H})^{-1} \sum_i \mathbf{v}_i (\mathbf{v}_i^T \mathbf{f}) \quad (28)$$

$$= \sum_i (\lambda\mathbf{I} - \mathbf{H})^{-1} \mathbf{v}_i (\mathbf{v}_i^T \mathbf{f}) \quad (29)$$

$$= \sum_i \frac{1}{\lambda - \mu_i} \mathbf{v}_i (\mathbf{v}_i^T \mathbf{f}) \quad (30)$$

and

$$\|\mathbf{x}\|^2 = \sum_i \left(\frac{1}{\lambda - \mu_i} \right)^2 (\mathbf{v}_i^T \mathbf{f})^2, \quad (31)$$

where the terms $\mathbf{v}_i^T \mathbf{f}$ and $(\mathbf{v}_i^T \mathbf{f})^2$ are constant for each quadratic form and can be computed in advance. The last equation also shows that the norm of \mathbf{x} is monotonically decreasing in the considered interval, so that there is exactly one solution and the search can be efficiently performed by a bisection method. \mathbf{x}^- can be found in the same way by maximizing the negative of g . Table 2 contains the pseudo-code of an algorithm that implements all the considerations above. A Matlab version can be downloaded from the authors' homepages.

If the matrix \mathbf{H} is negative definite (i.e. all its eigenvalues are negative) there is a global maximum that may not lie on the sphere, which might be used in substitution for \mathbf{x}^+ if it lies in a region of the input space that has a high probability of being reached (the criterion is quite arbitrary, but the region could be chosen to include, for example, 75% of the input data with highest density). The gradient of the function disappears at the global extremum such that it can be found by solving a simple linear equation system:

$$\nabla g(\mathbf{x}) = \mathbf{H}\mathbf{x} + \mathbf{f} = \mathbf{0} \quad (32)$$

$$\Leftrightarrow \mathbf{x} = -\mathbf{H}^{-1}\mathbf{f}. \quad (33)$$

In the same way a positive definite matrix \mathbf{H} has a negative global minimum, which might be used in substitution for \mathbf{x}^- .

For general nonlinear functions, the optimal stimuli can be found by standard techniques like gradient descent or stochastic methods (see e.g. Bishop, 1995, chap. 7). This is also useful for quadratic forms if there are additional constraints which are difficult to incorporate analytically (e.g. the non-negativity of the elements of \mathbf{x}^+). In Section 5 we provide an explicit formula for the gradient and the second derivative of g restricted to the sphere of vectors of fixed energy that can be used in such situations. A well-known drawback of online optimization algorithms is that they can get trapped in local extrema, depending on the point from which the algorithm started. In this context, the vector in the input data set that yields the largest output of g can be a good starting point.

In Figure 3 we show the optimal stimuli for the first 48 quadratic forms in the model system. In almost all cases \mathbf{x}^+ looks like a Gabor wavelet, in agreement with physiological data for neurons of the primary visual cortex (Pollen and Ronner, 1981; Adelson and Bergen, 1985; Jones and Palmer, 1987). The functions respond best to oriented stimuli having the same frequency as \mathbf{x}^+ . \mathbf{x}^- is usually structured as well and looks like a Gabor wavelet, too, which suggests that inhibition plays an important role. \mathbf{x}^+ can be used to compute the position and size of the receptive fields as well as the preferred orientation and frequency of the units for successive experiments.

Note that although \mathbf{x}^+ is the stimulus that elicits the strongest response in the function, it doesn't necessarily mean that it is representative of the class of stimuli that give the most important contribution to its output. This depends on the distribution of the input vectors: if \mathbf{x}^+ lies in a low-density region of the input space, it is possible that other kinds of stimuli drive the function more often. In that case they might be considered more relevant than \mathbf{x}^+ to characterize the function. Symptomatic for this effect would be if the output of a function when applied to its optimal stimulus would lie far outside the range of normal activity. This means that \mathbf{x}^+ can be an atypical, artificial input that pushes the function in an uncommon state. A similar effect has also been reported in some physiological papers comparing the response of neurons to natural stimuli and to artificial stimuli such as sine gratings (Baddeley et al., 1997). Thus the characterization of a neuron or a nonlinear function as a feature detector via the optimal stimulus

```

input: H, f, c: quadratic form
       r: norm of the solution (> eps)
       eps: tolerance of norm(x) from r

output: x_max: optimal excitatory stimulus x+

1- compute the eigenvalues mu(1) ... mu(N)
1- and the eigenvectors v(1) ... v(N) of H
2- # compute the coefficients of the eigenvector decomposition of f (Eq. 28)
2- alpha(i) := v(i)'*f      (i = 1 ... N)

3- # compute the range of the parameter lambda (Eqs. 17 and 26)
3- lambda_left := max(mu)
4- lambda_right := norm(f)/r + max(mu)

   # search by bisection until norm(x)^2 = r^2
5- # norm_x_2 holds the value of norm(x)^2 at the current lambda
5- norm_x_2 := 0
6- while abs(sqrt(norm_x_2)-r) > eps:
7-   # bisect the interval
7-   lambda = (lambda_right-lambda_left)/2 + lambda_left
8-   # compute the eigenvalues of (lambda*I - H)^-1 (Eq. 19)
8-   beta(i) := 1/(lambda-mu(i))      (i = 1 ... N)
9-   # compute norm(x)^2 at lambda (Eq. 31)
9-   norm_x_2 = sum(beta(i)^2 * alpha(i)^2)
   # update the interval limits
10-  if norm_x_2 > r^2:
11-    lambda_left = lambda
12-  else:
13-    lambda_right = lambda

14- # lambda found, compute the solution (Eq. 30)
14- x_max = sum(beta(i)*v(i)*alpha(i))

```

Table 2 Algorithm to compute the optimal stimuli Pseudo-code of the algorithm that computes the optimal excitatory stimulus of the inhomogeneous quadratic form. In the code, \mathbf{A}' means “ \mathbf{A} transpose”. The algorithm can be used to compute the optimal inhibitory stimulus by calling it with the negative of the quadratic form.

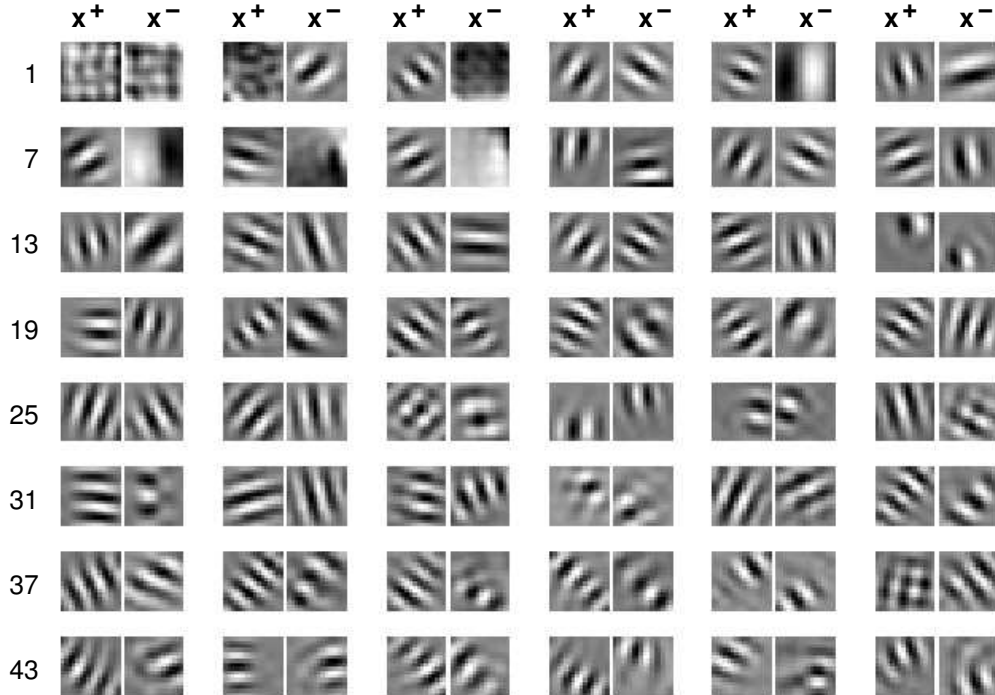


Figure 3 Optimal stimuli Optimal stimuli of the first 48 quadratic forms in the model system. \mathbf{x}^+ looks like a Gabor wavelet in almost all cases, in agreement with physiological data. \mathbf{x}^- is usually structured and is also similar to a Gabor wavelet, which suggests that inhibition plays an important role.

is at least incomplete (see also [MacKay, 1985](#)). However, the optimal stimuli remain extremely informative in practice.

5 Invariances

Since the considered functions are nonlinear, the optimal stimuli do not provide a complete description of their properties. We can gain some additional insights by studying a neighborhood of \mathbf{x}^+ and \mathbf{x}^- . An interesting question is, for instance, to which transformations of \mathbf{x}^+ or \mathbf{x}^- the function is invariant. This is similar to the common interpretation of neurons as detectors of a specific feature of the input which are invariant to a local transformation of that feature. For example, complex cells in the primary visual cortex are thought to respond to oriented bars and to be invariant to a local translation. In this section we are going to consider the function \tilde{g} , defined as g restricted to the sphere \mathcal{S} of radius r , since like in Section 4 we want to compare input vectors having fixed energy. Notice that although \tilde{g} and g take the same values on \mathcal{S} (i.e. $\tilde{g}(\mathbf{x}) = g(\mathbf{x})$ for each $\mathbf{x} \in \mathcal{S}$) they are two distinct mathematical objects. For example, the gradient of \tilde{g} in \mathbf{x}^+ is zero because \mathbf{x}^+ is by definition a maximum of \tilde{g} . On the other hand, the gradient of g in the same point is $\mathbf{H}\mathbf{x}^+ + \mathbf{f}$, which is in general different from zero.

Strictly speaking, there is no invariance in \mathbf{x}^+ , since it is a maximum and the output of \tilde{g} decreases in all directions (except in the special case where the linear term is zero and the first two or more eigenvalues are equal). In a general non-critical point \mathbf{x}^* (i.e. a point where the gradient does not disappear) the rate of change in any direction \mathbf{w} is given by its inner product with the gradient, $\nabla\tilde{g}(\mathbf{x}^*) \cdot \mathbf{w}$. For all vectors orthogonal to the gradient (which span an $N - 2$ dimensional space) the rate of change is thus zero. Note that this is not merely a consequence of the fact that the gradient is a first-order approximation of \tilde{g} . By the implicit function theorem (see e.g. [Walter, 1995](#), Theorem 4.5), in each open neighborhood U of a non-critical point \mathbf{x}^* there is an $N - 2$ dimensional level surface $\{\mathbf{x} \in U \subset \mathcal{S} \mid \tilde{g}(\mathbf{x}) = \tilde{g}(\mathbf{x}^*)\}$, since the domain of \tilde{g} (the sphere \mathcal{S}) is an $N - 1$ dimensional surface and its range (\mathbb{R}) is 1 dimensional. Each non-critical point thus belongs to an $N - 2$ dimensional surface where the value of the \tilde{g} stays constant. This is a somewhat surprising result: for an optimal stimulus there does not exist any invariance (except in some degenerate

cases); for a general sub-optimal stimulus there exist many invariances.

This shows that although it might be useful to observe for example that a given function f that maps images to real values is invariant to stimulus rotation, one should keep in mind that in a generic point there are a large number of other transformations to which the function might be equally invariant but that would lack an easy interpretation. The strict concept of invariance is thus not useful for our analysis, since in the extrema we have no invariances at all, while in a general point they are the typical case, and the only interesting direction is the one of maximal change, as indicated by the gradient. In the extremum \mathbf{x}^+ , however, since the output changes in all directions, we can relax the definition of invariance and look for the transformation to which the function changes as little as possible, as indicated by the direction with the smallest absolute value of the second derivative. (In a non-critical point this weak definition of invariance still does not help: if the quadratic form that represents the second derivative has positive as well as negative eigenvalues, there is still a $N - 3$ dimensional surface where the second derivative is zero.)

To study the invariances of the function g in a neighborhood of its optimal stimulus respecting the fixed energy constraint we have defined the function \tilde{g} as the function g restricted to \mathcal{S} . This is particularly relevant here since we want to analyze the derivatives of the function, i.e. its change under small movements. Any straight movement in space is going to leave the surface of the sphere. We must therefore be able to define movements on the sphere itself. This can be done by considering a path $\varphi(t)$ on the surface of \mathcal{S} such that $\varphi(0) = \mathbf{x}^+$ and then studying the change of g along φ . By doing this, however, we add the rate of change of the path (i.e. its acceleration) to that of the function. Of all possible paths we must take the ones that have as little acceleration as possible, i.e. those that have just the acceleration that is needed to stay on the surface. Such a path is called a *geodesic*. The geodesics of a sphere are great circles and our paths are thus defined as

$$\varphi(t) = \cos(t/r) \cdot \mathbf{x}^+ + \sin(t/r) \cdot r\mathbf{w} \quad (34)$$

for each direction \mathbf{w} in the tangential space of \mathcal{S} in \mathbf{x}^+ (i.e. for each \mathbf{w} orthogonal to \mathbf{x}^+), as shown in Figure 4. The $1/r$ factor in the cosine and sine arguments normalizes the function such that $\frac{d}{dt}\varphi(0) = \mathbf{w}$ with $\|\mathbf{w}\| = 1$.

The first derivative of \tilde{g} along φ is

$$\frac{d}{dt}(\tilde{g} \circ \varphi)(t) = \frac{d}{dt} \left[\frac{1}{2} \varphi(t)^T \mathbf{H} \varphi(t) + \mathbf{f}^T \varphi(t) + c \right] = \quad (35)$$

$$= \frac{d}{dt} \left[\frac{1}{2} (\cos(t/r) \mathbf{x}^+ + \sin(t/r) r\mathbf{w})^T \mathbf{H} (\cos(t/r) \mathbf{x}^+ + \sin(t/r) r\mathbf{w}) \right. \\ \left. + \mathbf{f}^T (\cos(t/r) \mathbf{x}^+ + \sin(t/r) r\mathbf{w}) + c \right] \quad (36)$$

$$= \frac{d}{dt} \left[\frac{1}{2} \cos(t/r)^2 \mathbf{x}^{+T} \mathbf{H} \mathbf{x}^+ + \cos(t/r) \sin(t/r) r \mathbf{x}^{+T} \mathbf{H} \mathbf{w} + \frac{1}{2} \sin(t/r)^2 r^2 \mathbf{w}^T \mathbf{H} \mathbf{w} \right. \\ \left. + \cos(t/r) \mathbf{f}^T \mathbf{x}^+ + \sin(t/r) r \mathbf{f}^T \mathbf{w} + c \right] \quad (37)$$

(since $\mathbf{w} \mathbf{H} \mathbf{x}^{+T} = \mathbf{x}^{+T} \mathbf{H} \mathbf{w}$, because \mathbf{H} is symmetric)

$$= -\frac{1}{r} \sin(t/r) \cos(t/r) \mathbf{x}^{+T} \mathbf{H} \mathbf{x}^+ + \cos(2t/r) \mathbf{x}^{+T} \mathbf{H} \mathbf{w} + \sin(t/r) \cos(t/r) r \mathbf{w}^T \mathbf{H} \mathbf{w} \\ - \frac{1}{r} \sin(t/r) \mathbf{f}^T \mathbf{x}^+ + \cos(t/r) \mathbf{f}^T \mathbf{w}. \quad (38)$$

Taking the second derivative we obtain

$$\frac{d^2}{dt^2}(\tilde{g} \circ \varphi)(t) = -\frac{1}{r^2} \cos(2t/r) \mathbf{x}^{+T} \mathbf{H} \mathbf{x}^+ - \frac{2}{r} \sin(2t/r) \mathbf{x}^{+T} \mathbf{H} \mathbf{w} + \cos(2t/r) \mathbf{w}^T \mathbf{H} \mathbf{w} \\ - \frac{1}{r^2} \cos(t/r) \mathbf{f}^T \mathbf{x}^+ - \frac{1}{r} \sin(t/r) \mathbf{f}^T \mathbf{w}. \quad (39)$$

In $t = 0$ we have

$$\frac{d^2}{dt^2}(\tilde{g} \circ \varphi)(0) = \mathbf{w}^T \mathbf{H} \mathbf{w} - \frac{1}{r^2} (\mathbf{x}^{+T} \mathbf{H} \mathbf{x}^+ + \mathbf{f}^T \mathbf{x}^+), \quad (40)$$

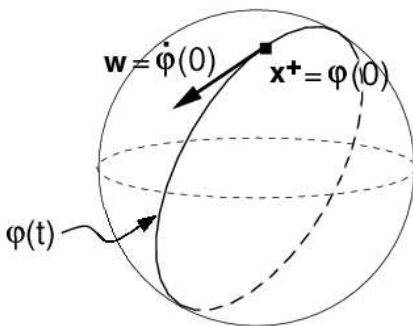


Figure 4 Geodetics on a sphere To compute the second derivative of the quadratic form on the surface of the sphere one can study the function along special paths on the sphere, known as geodetics. Geodetics of a sphere are great circles.

i.e. the second derivative of \tilde{g} in \mathbf{x}^+ in the direction of \mathbf{w} is composed of two terms: $\mathbf{w}^T \mathbf{H} \mathbf{w}$ corresponds to the second derivative of g in the direction of \mathbf{w} , while the constant term $-1/r^2 \cdot (\mathbf{x}^{+T} \mathbf{H} \mathbf{x}^+ + \mathbf{f}^T \mathbf{x}^+)$ depends on the curvature of the sphere $1/r^2$ and on the gradient of g in \mathbf{x}^+ orthogonally to the surface of the sphere:

$$\nabla g(\mathbf{x}^+) \cdot \mathbf{x}^+ = (\mathbf{H} \mathbf{x}^+ + \mathbf{f})^T \mathbf{x}^+ \quad (41)$$

$$= \mathbf{x}^{+T} \mathbf{H} \mathbf{x}^+ + \mathbf{f}^T \mathbf{x}^+. \quad (42)$$

To find the direction in which \tilde{g} decreases as little as possible we only need to minimize the absolute value of the second derivative (Eq. 40). This is equivalent to maximizing the first term $\mathbf{w}^T \mathbf{H} \mathbf{w}$ in (40), since the second derivative in \mathbf{x}^+ is always negative (because \mathbf{x}^+ is a maximum of \tilde{g}) and the second term is constant. \mathbf{w} is orthogonal to \mathbf{x}^+ and thus the maximization must be performed in the space tangential to the sphere in \mathbf{x}^+ . This can be done by computing a basis $\mathbf{b}_2, \dots, \mathbf{b}_N$ of the tangential space (for example using the Gram-Schmidt orthogonalization on $\mathbf{x}^+, \mathbf{e}_1, \dots, \mathbf{e}_{N-1}$ where \mathbf{e}_i is the canonical basis of \mathbb{R}^N) and replacing the matrix \mathbf{H} by

$$\tilde{\mathbf{H}} = \mathbf{B}^T \mathbf{H} \mathbf{B}, \quad (43)$$

where $\mathbf{B} = (\mathbf{b}_2, \dots, \mathbf{b}_N)$. The direction of smallest second derivative corresponds to the eigenvector $\tilde{\mathbf{v}}_1$ of $\tilde{\mathbf{H}}$ with the largest positive eigenvalue. The eigenvector must then be projected back from the tangential space into the original space by a multiplication with \mathbf{B} :

$$\mathbf{w}_1 = \mathbf{B} \tilde{\mathbf{v}}_1. \quad (44)$$

The remaining eigenvectors corresponding to eigenvalues of decreasing value are also interesting, as they point in orthogonal directions where the function changes with gradually increasing rate of change.

To visualize the invariances, we move \mathbf{x}^+ (or \mathbf{x}^-) along a path on the sphere in the direction of a vector \mathbf{w}_i according to

$$\mathbf{x}(\alpha) = \cos(\alpha) \mathbf{x}^+ + \sin(\alpha) r \mathbf{w}_i \quad (45)$$

for $\alpha \in [-\frac{\pi}{2}, \frac{\pi}{2}]$ as illustrated in Figure 5. At each point we measure the response of the function to the new input vector, and stop when it drops under 80% of the maximal response. In this way we generate for each invariance a movie like those shown in Figure 6 for some of the optimal stimuli (the corresponding animations are available at the authors' homepages). Each frame of such a movie contains a nearly-optimal stimulus. Using this analysis we can systematically scan a neighborhood of the optimal stimuli, starting from the transformations to which the function is most insensitive up to those that lead to a great change in response. Note that our definition of invariance applies only locally to a small neighborhood of \mathbf{x}^+ . The path followed in (45) goes beyond such a neighborhood and is appropriate only for visualization. Table 3 contains the pseudo-code of an algorithm that computes and visualizes the invariances of the optimal stimuli. A Matlab version can be downloaded from the authors' homepages.

```

input: H, f, c: quadratic form
       x_max: optimal excitatory stimulus  $x^+$ 
       dalpha: precision (angular step in degrees on the sphere for each frame
                of the invariance movies)

output: w(1) ... w(N-1) directions of the invariances, sorted by increasing
        magnitude of the second derivative
        nu(1) ... nu(N-1) value of the second derivative in the directions
        w(1) ... w(N-1)

1- # determine the radius of the sphere
1- r := norm(x_max)

2- # find a basis for the tangential plane of the sphere in  $x^+$ 
2- # e(1) ... e(N) is the canonical basis for  $R^N$ 
2- perform a Gram-Schmidt orthogonalization on x_max, e(1), ..., e(N-1) and
2- save the results in b(1) ... b(N)

# restrict the matrix H to the tangential plane
3- B := matrix with b(2) ... b(N) as columns
4- Ht := B'*H*B
# compute the invariances
5- compute the eigenvalues nu(1) ... nu(N-1) and the eigenvectors
5- w(1) ... w(N-1) of Ht, sorted by decreasing nu(i)
6- # compute the second derivative in the direction of the eigenvectors (Eq. 40)
6- nu(i) := nu(i) - 1/r^2 * (x_max'*H*x_max + f'*x_max)
7- # project the eigenvectors back to  $R^N$ 
7- w(i) := B*w(i)

8- # compute the value of the function at the maximum
8- out0 := 0.5*x_max'*H*x_max + f'*x_max + c
9- # minimal threshold value (80 percent of the maximum)
9- minout := 0.8*out0
# visualize the invariances (Eq. 45)
10- for i from 1 to N-1:
11-   out := out0
12-   alpha := 0
13-   x := x_max
14-   while out > minout:
15-     visualize x
16-     alpha := alpha + dalpha
17-     x := cos(alpha)*x_max + sin(alpha)*r*w(i)
18-     out := 0.5*x'*H*x + f'*x + c

19- repeat the visualization from step 10 with negative dalpha

```

Table 3 Algorithm to compute and visualize the invariances Pseudo-code of the algorithm that computes and visualizes the invariances of g in x^+ . In the code, \mathbf{A}' means “ \mathbf{A} transpose”.

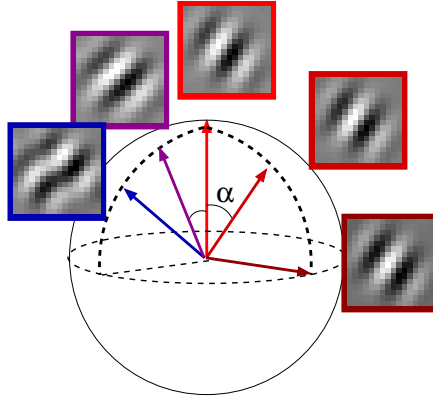


Figure 5 Visualization of the invariances This figure illustrates how the invariances are visualized. Starting from the optimal stimulus (top) we move on the sphere in the direction of an invariance until the response of the function drops below 80% of the maximal output or reaches 90 degrees. In the figure two invariances of Unit 4 are visualized. The one on the right represents a phase-shift invariance and preserves more than 80% of the maximal output until 90 degrees (the output at 90 degrees is 99.6% of the maximum). The one on the left represents an invariance to orientation change with an output that drops below 80% at 55 degrees.

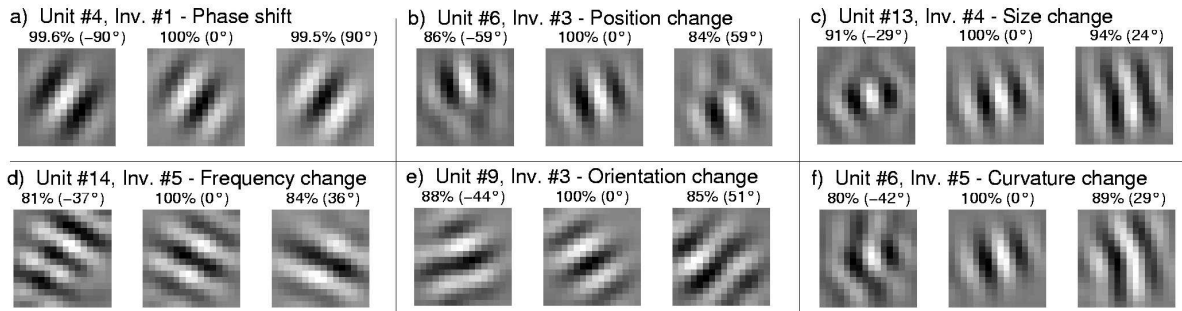


Figure 6 Invariance movies This figure shows selected invariances for some of the optimal excitatory stimuli shown in Fig. 3. The central patch of each plot represents the optimal stimulus of a quadratic form, while the ones on the sides are produced by moving it in the positive (right patch) or negative (left patch) direction of the eigenvector corresponding to the invariance. In this image, we stopped before the output dropped below 80% of the maximum to make the interpretation of the invariances easier. The relative output of the function in percent and the angle of displacement α (Eq. 45) are given above the patches. The animations corresponding to these invariances are available at the authors' homepages.

6 Significant invariances

The procedure described above finds for each optimal stimulus a set of $N - 1$ invariances ordered by the degree of invariance (i.e. by increasing magnitude of the second derivative). We would like to know which of these are statistically significant. An invariance can be defined to be significant if the function changes exceptionally little (less than chance level) in that direction, which can be measured by the value of the second derivative: the smaller its absolute value, the slower the function will change.

To test for their significance, we compare the second derivatives of the invariances of the quadratic form we are considering with those of random inhomogeneous quadratic forms that are equally adapted to the statistics of the input data. We therefore constrain the random quadratic forms to produce an output that has the same variance and mean as the output of the analyzed ones, when applied to the input stimuli. Without loss of generality, we assume here zero mean and unit variance. These constraints are compatible with the ones that are usually imposed to the functions learned by many theoretical models. Because of

this normalization, the distribution of the random quadratic forms depends on the distribution of the input data.

To understand how to efficiently build random quadratic forms under these constraints, it is useful to think in terms of a dual representation of the problem. A quadratic form over the input space is equivalent to a linear function over the space of the input expanded to all monomials of degree one and two using the function $\Phi((x_1, \dots, x_n)^T) := (x_1x_1, x_1x_2, x_1x_3, \dots, x_nx_n, x_1, \dots, x_n)^T$, i.e.

$$\frac{1}{2} \mathbf{x}^T \underbrace{\begin{pmatrix} h_{11} & h_{12} & \cdots & h_{1n} \\ h_{12} & h_{22} & & \\ \vdots & & \ddots & \vdots \\ h_{1n} & \cdots & & h_{nn} \end{pmatrix}}_{\mathbf{H}} \mathbf{x} + \underbrace{\begin{pmatrix} f_1 \\ f_2 \\ \vdots \\ f_n \end{pmatrix}}_{\mathbf{f}}^T \mathbf{x} + c = \underbrace{\begin{pmatrix} \frac{1}{2}h_{11} \\ h_{12} \\ h_{13} \\ \vdots \\ \frac{1}{2}h_{nn} \\ f_1 \\ \vdots \\ f_n \end{pmatrix}}_{\mathbf{q}}^T \underbrace{\begin{pmatrix} x_1x_1 \\ x_1x_2 \\ x_1x_3 \\ \vdots \\ x_nx_n \\ x_1 \\ \vdots \\ x_n \end{pmatrix}}_{\Phi(\mathbf{x})} + c. \quad (46)$$

We can whiten the *expanded* input data $\Phi(\mathbf{x})$ by subtracting its mean $\langle \Phi(\mathbf{x}) \rangle_t$ and transforming it with a whitening matrix \mathbf{S} . In this new coordinate system, each linear filter with norm 1 fulfills the unit variance and zero mean constraints by construction. We can thus choose a random vector \mathbf{q}' of length 1 in the whitened, expanded space and derive the corresponding quadratic form in the original input space:

$$\mathbf{q}'^T (\mathbf{S}(\Phi(\mathbf{x}) - \langle \Phi(\mathbf{x}) \rangle_t)) = \underbrace{(\mathbf{S}^T \mathbf{q}')^T}_{=:\mathbf{q}} (\Phi(\mathbf{x}) - \langle \Phi(\mathbf{x}) \rangle_t) \quad (47)$$

$$= \mathbf{q}^T (\Phi(\mathbf{x}) - \langle \Phi(\mathbf{x}) \rangle_t) \quad (48)$$

$$\stackrel{(46)}{=} \frac{1}{2} \mathbf{x}^T \mathbf{H} \mathbf{x} + \mathbf{f}^T \mathbf{x} - \mathbf{q}^T \langle \Phi(\mathbf{x}) \rangle_t \quad (49)$$

$$= \frac{1}{2} \mathbf{x}^T \mathbf{H} \mathbf{x} + \mathbf{f}^T \mathbf{x} + c, \quad (50)$$

with appropriately defined \mathbf{H} and \mathbf{f} according to Equation (46).

We can next compute the optimal stimuli and the second derivative of the invariances of the obtained random quadratic form. To make sure that we get independent measurements we only keep one second derivative chosen at random for each random function. This operation, repeated over many quadratic forms, allows us to determine a distribution of the second derivatives of the invariances and a corresponding confidence interval.

Figure 7a shows the distribution of 50,000 independent second derivatives of the invariances of random quadratic forms and the distribution of the second derivatives of all invariances of the first 50 quadratic forms learned in the model system. The dashed line indicates the 95% confidence interval derived from the former distribution. The latter is more skewed towards small second derivatives and has a clear peak near zero. 28% of all invariances were classified to be significant. Figure 7b shows the number of significant invariances for each individual quadratic form in the model system. Each function has 49 invariances since the rank of the quadratic term is 50 (see Sect. 2). The plot shows that the number of significant invariances decreases with increasing ordinal number (the functions are ordered by slowness, the first ones being the slowest). 46 units out of 50 have 3 or more significant invariances. The first invariance, which corresponds to a phase shift invariance, was always classified as significant, which confirms that the units behave like complex cells. Note that since the eigenvalues of a quadratic form are not independent of each other, with the method presented here it is only possible to make statements about the significance of *individual* invariances, and not about the joint probability distribution of two or more invariances.

7 Relative contribution of the quadratic, linear, and constant term

The inhomogeneous quadratic form has a quadratic, a linear, and a constant term. It is sometimes of interest to know what their relative contribution to the output is. The answer to this question depends on

the considered input. For example, the quadratic term dominates for large input vectors while the linear or even the constant term dominates for input vectors with a small norm.

A first possibility is to look at the contribution of the individual terms at a particular point. A privileged point is, for example, the optimal excitatory stimulus, especially if the quadratic form can be interpreted as a feature detector (cf. Sect. 4). Figure 8a shows for each function in the model system the absolute value of the output of all terms with \mathbf{x}^+ as an input. In all functions except the first two, the activity of the quadratic term is greater than that of the linear and of the constant term. The first function basically computes the mean pixel intensity, which explains the dominance of the linear term. The second function is dominated by a constant term from which a quadratic expression very similar to the squared mean pixel intensity is subtracted.

As an alternative we can consider the ratio between linear and quadratic term, averaged over all input stimuli:

$$\left\langle \log \left(\frac{\mathbf{f}^T \mathbf{x}}{\frac{1}{2} \mathbf{x}^T \mathbf{H} \mathbf{x}} \right) \right\rangle_t = \langle \log(\mathbf{f}^T \mathbf{x}) - \log\left(\frac{1}{2} \mathbf{x}^T \mathbf{H} \mathbf{x}\right) \rangle_t. \quad (51)$$

The logarithm ensures that a given ratio (e.g. linear/quadratic = 3) has the same weight as the inverse ratio (e.g. linear/quadratic = 1/3) in the mean. A negative result means that the quadratic term dominates while for a positive value the linear term dominates. Figure 8b shows the histogram of this measure for the functions in the model system. In all but 4 units (Units 1, 7, 8, and 24) the quadratic term is on average greater than the linear one.

8 Quadratic forms without linear term

In the case of a quadratic form without the linear term, i.e.

$$g(\mathbf{x}) = \frac{1}{2} \mathbf{x}^T \mathbf{H} \mathbf{x} + c \quad (52)$$

the mathematics of Sections 4 and 5 becomes much simpler. The quadratic form is now centered at $\mathbf{x} = \mathbf{0}$, and the direction of maximal increase corresponds to the eigenvector \mathbf{v}_1 with the largest positive eigenvalue. The optimal excitatory stimulus \mathbf{x}^+ with norm r is thus

$$\mathbf{x}^+ = r \mathbf{v}_1. \quad (53)$$

Similarly, the eigenvector corresponding to the largest negative eigenvalue \mathbf{v}_N points in the direction of \mathbf{x}^- .

The second derivative (Eq. 40) in \mathbf{x}^+ in this case becomes

$$\frac{d^2}{dt^2}(\tilde{g} \circ \varphi)(0) = \mathbf{w}^T \mathbf{H} \mathbf{w} - \frac{1}{r^2} \mathbf{x}^{+T} \mathbf{H} \mathbf{x}^+ \quad (54)$$

$$= \mathbf{w}^T \mathbf{H} \mathbf{w} - \mathbf{v}_1^T \mathbf{H} \mathbf{v}_1 \quad (55)$$

$$= \mathbf{w}^T \mathbf{H} \mathbf{w} - \mu_1. \quad (56)$$

The vector \mathbf{w} is by construction orthogonal to \mathbf{x}^+ and lies therefore in the space spanned by the remaining eigenvectors $\mathbf{v}_2, \dots, \mathbf{v}_N$. Since μ_1 is the maximum value that $\mathbf{w}^T \mathbf{H} \mathbf{w}$ can assume for vectors of length 1 it is clear that (56) is always negative (as it should since \mathbf{x}^+ is a maximum) and that its absolute value is successively minimized by the eigenvectors $\mathbf{v}_2, \dots, \mathbf{v}_N$ in this order. The value of the second derivative for \mathbf{v}_i is given by

$$\frac{d^2}{dt^2}(\tilde{g} \circ \varphi)(0) = \mathbf{v}_i^T \mathbf{H} \mathbf{v}_i - \mu_1 \quad (57)$$

$$= \mu_i - \mu_1. \quad (58)$$

In the same way, the invariances of \mathbf{x}^- are given by $\mathbf{v}_{N-1}, \dots, \mathbf{v}_1$ with second derivative values $(\mu_i - \mu_N)$.

Quadratic forms without the linear term were analyzed in some recent theoretical (Hashimoto, 2003; Bartsch and Obermayer, 2003) and experimental (Touryan et al., 2002) studies. There, the eigenvectors of \mathbf{H} were visualized and interpreted as “relevant features”. Some of them were discarded because they were “unstructured”. According to our analysis, this interpretation only holds for the two eigenvectors with

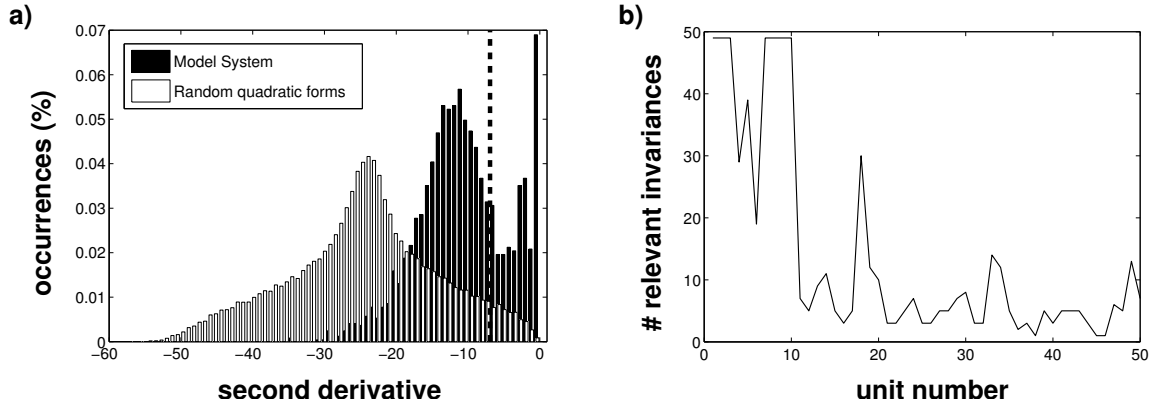


Figure 7 Significant invariances (a) Distribution of 50,000 independently drawn second derivatives of the invariances of random quadratic forms and distribution of the second derivatives of all invariances of the first 50 quadratic forms learned in the model system. The dashed line indicates the 95% confidence interval as derived from the random quadratic forms. The distribution in the model system is more skewed toward small second derivatives and has a clear peak near zero. 28% of all invariances were classified as significant. (b) Number of significant invariances for each of the first 50 quadratic forms learned in the model system (the functions were sorted by decreasing slowness, see Sect. 2). The number of significant invariances tends to decrease with decreasing slowness.

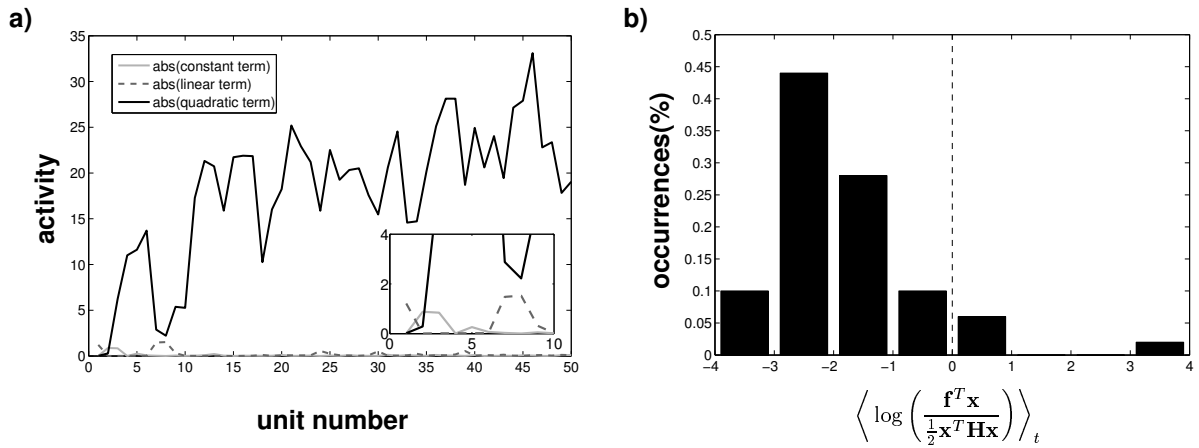


Figure 8 Relative contribution of the quadratic, linear, and constant term (a) This figure shows the absolute value of the output of the quadratic, linear and constant term in \mathbf{x}^+ for each of the first 50 functions in the model system. In all but the first 2 units the quadratic term has a larger output. The subplot shows a magnified version of the contribution of the terms for the first 10 units. (b) Histogram of the mean of the logarithm of the ratio between the activity of the linear and the quadratic term in the model system, when applied to 90,000 test input vectors. A negative value means that the quadratic term dominates while for a positive value the linear term dominates. In all but 4 units (Units 1, 7, 8, and 24) the quadratic term is on average greater.

largest positive and negative eigenvalues. We think that the remaining eigenvectors should not be visualized directly but applied as transformations to the optimal stimuli. Therefore it is possible for them to look unstructured but still represent a structured invariance, as illustrated in Figure 9. For example, Hashimoto (2003, Fig. 5a) shows in her paper the eigenvectors of a quadratic form learned by a variant of SFA performed by gradient descent. The two largest eigenvectors look like two Gabor wavelets and have the same orientation and frequency. According to the interpretation above and to the cited paper, this shows that the network responds best to an oriented stimulus and is invariant to a phase shift. The third eigenvector looks like a Gabor wavelet with the same frequency as the first two but a slightly different orientation. Hashimoto suggests that the eigenvector makes the interpretation of that particular quadratic form difficult (Hashimoto, 2003, page 777). According to our analysis, that vector might code for a rotation invariance, which would be compatible with a complex-cell behavior.

$$\cos(\alpha) \cdot \underbrace{\text{[stimulus]}}_{\mathbf{x}^+} + \sin(\alpha) \cdot \underbrace{\text{[stimulus]}}_{r \mathbf{w}} = \text{[stimulus]}$$

Figure 9 Interpretation of the invariances This figure illustrates the fact that although the vector corresponding to an invariance (center) might be difficult to interpret or even look unstructured, when applied to the optimal excitatory stimulus (left) it can code for a meaningful invariance (right). The invariance shown here is the curvature invariance of Fig. 6f.

Based on spike-triggered average (STA) Rust et al. (2004) computed the best linear approximation of the input-output function computed by some neurons. On the space orthogonal to that function they then determined the best quadratic approximation given by the spike-triggered covariance matrix. They interpreted the eigenvectors corresponding to the eigenvalues with largest absolute value as the basis that spans the subspace of stimuli that governs the response of a cell. Our analysis is consistent with this interpretation, since every stimulus that is generated by a linear combination of the optimal stimulus and the most relevant invariances is going to produce a strong output in the quadratic form.

9 Related neural networks

9.1 Decomposition of a quadratic form in a neural network

As also noticed by Hashimoto (2003), for each quadratic form there exists an equivalent two layer neural network, which can be derived by rewriting the quadratic form using its eigenvector decomposition:

$$g(\mathbf{x}) = \frac{1}{2} \mathbf{x}^T \mathbf{H} \mathbf{x} + \mathbf{f}^T \mathbf{x} + c \quad (59)$$

$$= \frac{1}{2} \mathbf{x}^T \mathbf{V} \mathbf{D} \mathbf{V}^T \mathbf{x} + \mathbf{f}^T \mathbf{x} + c \quad (60)$$

$$= \frac{1}{2} (\mathbf{V}^T \mathbf{x})^T \mathbf{D} (\mathbf{V}^T \mathbf{x}) + \mathbf{f}^T \mathbf{x} + c \quad (61)$$

$$= \sum_{i=1}^N \frac{\mu_i}{2} (\mathbf{v}_i^T \mathbf{x})^2 + \mathbf{f}^T \mathbf{x} + c. \quad (62)$$

One can thus define a neural network with a first layer formed by a set of N linear subunits $s_k(\mathbf{x}) = \mathbf{v}_k^T \mathbf{x}$ followed by a quadratic nonlinearity weighted by the coefficients $\mu_k/2$. The output neuron sums the contribution of all subunits plus the output of a direct linear connection from the input layer (Fig. 10a). Since the eigenvalues can be negative, some of the subunits give an inhibitory contribution to the output. It is interesting to note that in an algorithm that learns quadratic forms the number of inhibitory subunits in the equivalent neural network is not fixed but is a learned feature. As an alternative one can scale the weights

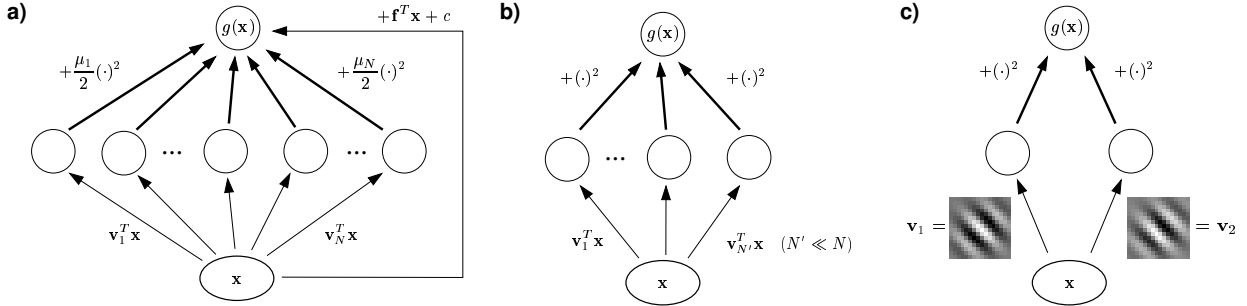


Figure 10 Neural networks related to inhomogeneous quadratic forms In all plots we assume that the norm of the subunits is normalized to 1, i.e. $\|\mathbf{v}_i\| = 1$. The ellipse in the input layer represents a multidimensional input. **(a)** Neural network equivalent to an inhomogeneous quadratic form. The first layer consists of linear subunits, followed by a quadratic nonlinearity weighted by the coefficients $\mu_i/2$. The output neuron sums the contribution of each subunit plus the output of a direct linear connection from the input layer. **(b)** Simpler neural network used in some theoretical studies. The output of the linear subunits is squared but not weighted and can only give an excitatory (positive) contribution to the output. There is no direct linear connection between input and output layer. **(c)** The energy model of complex cells consists of two linear subunits whose weights are Gabor filters having the same shape except for a 90° phase difference. The output is given by the square sum of the response of the two subunits.

\mathbf{v}_i by $\sqrt{|\mu_i|/2}$ and specify which subunits are excitatory and which are inhibitory according to the sign of μ_i , since

$$g(\mathbf{x}) \stackrel{(62)}{=} \sum_{i=1}^N \frac{\mu_i}{2} (\mathbf{v}_i^T \mathbf{x})^2 + \mathbf{f}^T \mathbf{x} + c \quad (63)$$

$$= \sum_{\substack{i=1 \\ \mu_i > 0}}^N \left(\left(\sqrt{\frac{|\mu_i|}{2}} \mathbf{v}_i \right)^T \mathbf{x} \right)^2 - \sum_{\substack{i=1 \\ \mu_i < 0}}^N \left(\left(\sqrt{\frac{|\mu_i|}{2}} \mathbf{v}_i \right)^T \mathbf{x} \right)^2 + \mathbf{f}^T \mathbf{x} + c. \quad (64)$$

This equation also shows that the subunits are unique only up to an orthogonal transformation (i.e. a rotation or reflection) of the excitatory subunits and another one of the inhibitory subunits, which can be seen as follows. Let \mathbf{A}^+ and \mathbf{A}^- be the matrices having as rows the vectors $\sqrt{|\mu_i|/2} \mathbf{v}_i$ for positive and negative μ_i , respectively. Equation (64) can then be rewritten as

$$g(\mathbf{x}) = \|\mathbf{A}^+ \mathbf{x}\|^2 - \|\mathbf{A}^- \mathbf{x}\|^2 + \mathbf{f}^T \mathbf{x} + c. \quad (65)$$

Since the length of a vector doesn't change under rotation or reflection, the output of the function remains unchanged if we introduce two orthogonal transformations \mathbf{R}^+ and \mathbf{R}^- :

$$g(\mathbf{x}) = \|\mathbf{R}^+ \mathbf{A}^+ \mathbf{x}\|^2 - \|\mathbf{R}^- \mathbf{A}^- \mathbf{x}\|^2 + \mathbf{f}^T \mathbf{x} + c. \quad (66)$$

Figure 11 shows the weights of the subunits of the neural network equivalent to one of the units learned in the model system as defined by the eigenvectors of \mathbf{H} (Eq. 62) and some examples of the weights after a random rotation of the excitatory and inhibitory subunits. The subunits are not as structured as in the case of the eigenvectors, although the orientation and frequency can still be identified.

The neural model suggests alternative ways to learn quadratic forms, for example by adapting the weights by backpropagation. The high number of parameters involved, however, could make it difficult for an incremental optimization method to avoid local extrema. On the other hand, each network of this form can be transformed into a quadratic form and analyzed with the techniques described in this paper, which might be useful for example to compute the optimal stimuli and the invariances.

9.2 Relation to some theoretical studies

Closely related neural networks were used in some theoretical studies (Hyvärinen and Hoyer, 2000; Hyvärinen and Hoyer, 2001; Körding et al., 2004). There, a small set of linear subunits (2 to 25) was connected to an

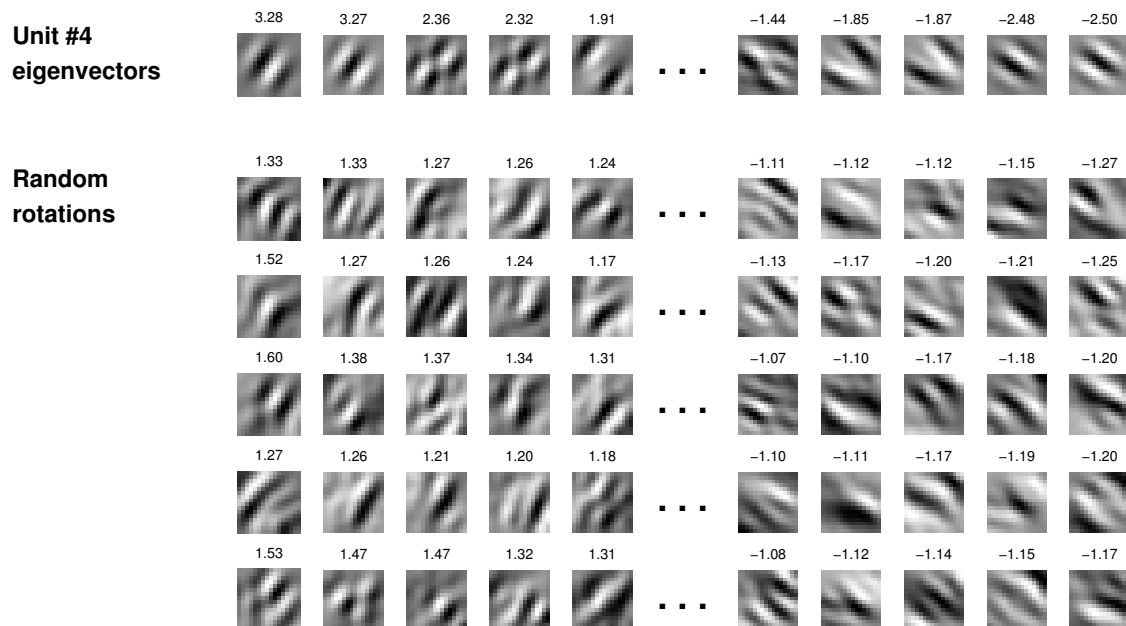


Figure 11 Random rotations of the positive and negative subunits The weights of the subunits of Unit 4 as defined by the eigenvectors of \mathbf{H} (Eq. 62) and five examples of the weights after a random rotation of the excitatory and inhibitory subunits. The numbers above the patches are the weighting coefficients on the second layer when the weight vectors of the first layer are normalized to 1.

output unit that took the sum of the squared activities (Fig. 10b). These networks differ from inhomogeneous quadratic forms in that they lack a direct linear contribution to the output and have much fewer subunits (a quadratic form of dimension N has N subunits). The most important difference, however, is related to the normalization of the weights. In the theoretical studies cited above the weights are normalized to a fixed norm and the activity of the subunits is not weighted. In particular, since there are no negative coefficients, no inhibition is possible.

9.3 Comparison with the hierarchical model of V1

The equivalent neural network shows that quadratic forms are compatible with the hierarchical model of the visual cortex first proposed by Hubel and Wiesel (1962), in which complex cells pool over simple cells having similar orientation and frequency in order to achieve phase-shift invariance. This was later formalized in the *energy model* of complex cells (Adelson and Bergen, 1985), which can be implemented by the neural network introduced above. The subunits are interpreted as simple cells and the output unit as a complex cell. In its usual description the energy model consists of only two excitatory subunits. If for example the subunits are two Gabor wavelets with identical envelope function, frequency, and orientation but with a 90° phase difference (Fig. 10c), the network will reproduce the basic properties of complex cells, i.e. edge detection and shift invariance. Additional excitatory or inhibitory subunits might introduce additional complex cell invariances, broaden or sharpen the orientation and frequency tuning, and provide end- or side-inhibition. However, as mentioned in the previous section the neural network is not unique, so that the subunits can assume different forms many of which might not be similar to simple cells (Fig. 11). For example, as discussed in Section 8, if the linear term is missing and the subunits are defined using the eigenvectors of \mathbf{H} as in Equation (62), the linear filters of the subunits can be interpreted as the optimal stimuli and the invariances thereof. As shown in Figure 11, the invariances themselves need not be structured like a simple cell, since they only represent transformations of the optimal stimuli.

10 Conclusion

In this paper we have presented a collection of tools to analyze nonlinear functions and in particular quadratic forms. These tools allow us to visualize the coefficients of the individual terms of an inhomogeneous quadratic form, to compute its optimal stimuli (i.e. the stimuli that maximize or minimize the quadratic form under a fixed energy constraint) and their invariances (i.e. the transformations of the optimal stimuli to which the quadratic form is most insensitive), and a method to determine which of these invariances are statistically significant. We have also proposed a way to measure the relative contribution of the linear and quadratic term. Moreover, we have discussed a neural network architecture equivalent to a given quadratic form. The methods presented here can be used in a variety of fields, in particular in physiological experiments to study the nonlinear receptive fields of neurons and in theoretical studies.

11 Additional material

The site <http://itb.biologie.hu-berlin.de/~berkes/qforms/index.shtml> contains additional material to this paper, including the animations corresponding to Figure 6 and Matlab source code for the algorithms of Table 2 and 3.

12 Acknowledgments

This work has been supported by a grant from the Volkswagen Foundation. We are grateful to Thomas Neukircher for some very interesting discussions about some of the mathematical ideas of the paper and to Henning Sprekeler for revising the manuscript.

References

- Adelson, E. H. and Bergen, J. R. (1985). Spatiotemporal energy models for the perception of motion. *Journal Optical Society of America A*, 2(2):284–299. 7, 19
- Baddeley, R., Abbott, L., Booth, M., Sengpiel, F., Freeman, T., Wakeman, E., and Rolls, E. (1997). Responses of neurons in primary and inferior temporal visual cortices to natural scenes. *Proc R Soc Lond B Biol Sci.*, 264(1389):1775–83. 7
- Bartsch, H. and Obermayer, K. (2003). Second-order statistics of natural images. *Neurocomputing*, 52–54:467–472. 15
- Berkes, P. and Wiskott, L. (2002). Applying slow feature analysis to image sequences yields a rich repertoire of complex cell properties. In Dorransoro, J. R., editor, *Artificial Neural Networks - ICANN 2002 Proceedings*, Lecture Notes in Computer Science, pages 81–86. Springer. 1, 2
- Berkes, P. and Wiskott, L. (2003). Slow feature analysis yields a rich repertoire of complex-cell properties. Cognitive Sciences EPrint Archive (CogPrint) 2804, <http://cogprints.ecs.soton.ac.uk/archive/00002804/>. 1, 3
- Bishop, C. M. (1995). *Neural Networks for Pattern Recognition*. Oxford University Press. 7
- Dayan, P. and Abbott, L. F. (2001). *Theoretical neuroscience: computational and mathematical modeling of neural systems*. The MIT Press. 5
- Fortin, C. (2000). A survey of the trust region subproblem within a semidefinite framework. Master’s thesis, University of Waterloo. 5, 6
- Hashimoto, W. (2003). Quadratic forms in natural images. *Network: Computation in Neural Systems*, 14(4):765–788. 15, 17
- Hubel, D. and Wiesel, T. (1962). Receptive fields, binocular interaction and functional architecture in the cat’s visual cortex. *Journal of Physiology*, 160:106–154. 19

- Hyvärinen, A. and Hoyer, P. (2000). Emergence of phase and shift invariant features by decomposition of natural images into independent feature subspaces. *Neural Computation*, 12(7):1705–1720. 18
- Hyvärinen, A. and Hoyer, P. (2001). A two-layer sparse coding model learns simple and complex cell receptive fields and topography from natural images. *Vision Research*, 41(18):2413–2423. 18
- Jones, J. P. and Palmer, L. A. (1987). An evaluation of the two-dimensional Gabor filter model of simple receptive fields in cat striate cortex. *Journal of Neurophysiology*, 58(6):1233–1257. 7
- Jutten, C. and Karhunen, J. (2003). Advances in nonlinear blind source separation. *Proc. of the 4th Int. Symp. on Independent Component Analysis and Blind Signal Separation (ICA2003)*, pages 245–256. 1
- Körding, K., Kayser, C., Einhäuser, W., and König, P. (2004). How are complex cell properties adapted to the statistics of natural scenes? *Journal of Neurophysiology*, 91(1):206–212. 18
- MacKay, D. (1985). The significance of "feature sensitivity". In Rose, D. and Dobson, V., editors, *Models of the visual cortex*, pages 47–53. John Wiley & Sons Ltd. 9
- Pollen, D. and Ronner, S. (1981). Phase relationship between adjacent simple cells in the visual cortex. *Science*, 212:1409–1411. 7
- Rust, N. C., Schwartz, O., Moxshon, J. A., and Simoncelli, E. (2004). Spike-triggered characterization of excitatory and suppressive stimulus dimensions in monkey V1. *Neurocomputing*, 58–60:793–799. 1, 17
- Schölkopf, B., Smola, A., and Müller, K.-R. (1998). Nonlinear component analysis as a kernel eigenvalue problem. *Neural Computation*, 10(5):1299–1319. 1
- Stork, D. and Levinson, J. (1982). Receptive fields and the optimal stimulus. *Science*, 216:204–205. 5
- Touryan, J., Lau, B., and Dan, Y. (2002). Isolation of relevant visual features from random stimuli for cortical complex cells. *Journal of Neuroscience*, 22(24):10811–10818. 1, 15
- Walter, W. (1995). *Analysis 2*. Springer Verlag. 9
- Wiskott, L. and Sejnowski, T. (2002). Slow feature analysis: Unsupervised learning of invariances. *Neural Computation*, 14(4):715–770. 1, 3